Biochimica et Biophysica Acta 1787 (2009) 272–279

Contents lists available at ScienceDirect

Biochimica et Biophysica Acta

journal homepage: www.elsevier.com/locate/bbabio

Structural organisation of phycobilisomes from *Synechocystis* sp. strain PCC6803 and their interaction with the membrane☆

Ana A. Arteni [a,b], Ghada Ajlani [b], Egbert J. Boekema [a,*]

[a] Department of Biophysical Chemistry, University of Groningen, Nijenborgh 4, 9747 AG Groningen, The Netherlands
[b] Institut de Biologie et de Technologies de Saclay, Centre National de la Recherche Scientifique, Commissariat à l'Energie Atomique, 91191 Gif-sur-Yvette, France

ARTICLE INFO

Article history:
Received 14 November 2008
Received in revised form 14 January 2009
Accepted 15 January 2009
Available online 22 January 2009

Keywords:
Cyanobacteria
Phycobilisome
Ferredoxin
NADP oxidoreductase
Electron microscopy
Negative staining
Single particle image analysis

ABSTRACT

In cyanobacteria, the harvesting of light energy for photosynthesis is mainly carried out by the phycobilisome — a giant, multi-subunit pigment–protein complex. This complex is composed of heterodimeric phycobiliproteins that are assembled with the aid of linker polypeptides such that light absorption and energy transfer to photosystem II are optimised. In this work we have studied, using single particle electron microscopy, the phycobilisome structure in mutants lacking either two or all three of the phycocyanin hexamers. The images presented give much greater detail than those previously published, and in the best two-dimensional projection maps a resolution of 13 Å was achieved. As well as giving a better overall picture of the assembly of phycobilisomes, these results reveal new details of the association of allophycocyanin trimers within the core. Insights are gained into the attachment of this core to the membrane surface, essential for efficient energy transfer to photosystem II. Comparison of projection maps of phycobilisomes with and without reconstituted ferredoxin:NADP oxidoreductase suggests a location for this enzyme within the complex at the rod-core interface.

1. Introduction

Cyanobacteria and chloroplasts are defined by their ability to carry out oxygenic photosynthesis, using two highly-conserved photosystems located in the thylakoid membrane. In place of the intra-membranous antennae found in most chloroplasts (and some cyanobacteria), light-harvesting in cyanobacteria and several groups of eukaryotic algae is principally performed by giant soluble complexes associated with the membrane surface, called phycobilisomes (PBS). Although a PBS is composed of hundreds of phycobiliproteins plus a few linker polypeptides, light energy absorbed anywhere within the particle is efficiently transferred towards the photosystems within the membrane [1].

A phycobiliprotein is composed of two polypeptide subunits (α and β), each covalently binding an open-chain tetrapyrrole chromophore known as a phycobilin. The αβ heterodimer assembles into disc-like trimers $(\alpha\beta)_3$ or hexamers $(\alpha\beta)_6$, which possess a central cavity. Linker polypeptides are believed to bind in the central cavity of the phycobiliprotein discs [2,3]. The core of the PBS, composed of trimeric $(\alpha\beta)_3$ discs of allophycocyanin (AP) stacked into cylinders, forms a physical connection with the stromal surface of the photosynthetic membrane. A series of rods, comprising cylinders of stacked hexameric $(\alpha\beta)_6$ discs, radiate from the core. Different linkers are specifically responsible for each level of phycobiliprotein assembly and function to stabilise the PBS and optimise its absorption and energy transfer characteristics (Fig. 1).

High-resolution X-ray diffraction structures have been determined for various types of PBS components. For example, in the crystal structure of the allophycocyanin core protein from the red alga *Porphyra yezoensis* two trimers are loosely stacked together in the unit cell to form a disc of diameter 105.3 Å and thickness 63.1 Å [4]. C-phycocyanin from the cyanobacterium *Synechococcus elongatus* is a hexameric disc of 110 Å diameter by 60 Å thickness [5]. While many isolated components of different PBSs have been crystallised, the structure of the entire PBS and the manner of its association with photosystem II can only be suggested. Based on the overall structure of PBSs as visualized by electron microscopy (EM), several distinct morphological PBS families have been described. The most common and best-described family is the hemi-discoidal PBSs, found in several cyanobacteria, rhodophytes and the glaucophyte *Cyanophora paradoxa* [6]. Another family comprises the hemi-ellipsoidal PBSs, which appear to have a substantially larger width. They were originally found in the red alga *Porphyridium cruentum* [7], and are also present in some cyanobacteria. A unique bundle-shaped PBS has been described for the cyanobacterium *Gloeobacter violaceus* [8,9].

The hemi-discoidal PBS family has been further divided into three subgroups according to structural differences of the core domain [6].

Abbreviations: EM, electron microscopy; AP, allophycocyanin; PC, phycocyanin; PBS, phycobilisome; L_X, linker polypeptide located at position X of the PBS, where X can be C (core), R (rod), RC (rod core) or CM (core membrane)

☆ Linkers with identical location are distinguished by a superscript just above the X indicating their molecular mass.

* Corresponding author. Tel.: +31 50 3634225; fax: +31 50 3634800.
E-mail address: e.j.boekema@rug.nl (E.J. Boekema).

0005-2728/$ – see front matter © 2009 Elsevier B.V. All rights reserved.
doi:10.1016/j.bbabio.2009.01.009

This domain is composed of 2, 3 or 5 cylinders of stacked allophycocyanin trimers. Bi-cylindrical cores are exemplified by *Synechococcus* sp. PCC 6301 [10]. Tri-cylindrical cores have been observed in several cyanobacteria such as *Synechococcus* sp. PCC7002 [11], *Synechocystis* spp. PCC6701 and PCC6803 [12,13], but are also found in the red algae *Porphyridium cruentum* [14]. Penta-cylindrical cores, as exemplified by *Mastigocladus laminosus* and *Anabaena* sp. PCC7120 [15,16], appear to be less common.

Each of the cylinders belonging to the core substructure is composed of four trimeric AP discs (apart from the extra two cylinders in penta-cylindrical cores which have only two discs), and these discs have slightly different compositions (Fig. 1). The upper cylinder (not present in bi-cylindrical cores) is composed of two simple AP trimers $(\alpha\beta)_3$ that we will call T, and two other discs we designate T8 (T plus L_C, a linker of 8 kDa). The two basal cylinders are composed of one T disc, one T8 disc, one disc we designate B8 (T8 with one α-subunit replaced by an isoform called AP-B) and one M disc (T with one αβ heterodimer replaced by a red-shifted β isoform, β18, plus a domain of the linker L_{CM} for α) [17]. The core-membrane linker L_{CM}, the major linker polypeptide in the core, is responsible for the assembly of AP discs into cylinders, and of cylinders together to form the core. L_{CM} also plays a key role in anchoring the PBS to the photosynthetic membrane (possibly via direct interaction with PSII), and in tuning the properties of the bound pigment cofactors (phycobilins) such that absorbed light energy is funnelled towards the photosystems. Two copies of this multifunctional polypeptide (mass 75–125 kDa) are present per PBS core. The L_{CM} polypeptide is divided into several domains (Fig. 1). The C-terminal portion of the L_{CM} contains two to four repeated domains (Rep), depending on the organism, each of about 120 residues. The Reps are ~60% similar to the conserved domains of the rod linkers (L_R) and are likely to play the same role (i.e. interaction between discs in a cylinder) [18]. The number of Reps determines the cylinder number in the core structure. The N-terminal portion of L_{CM} (the PB domain) is 55% similar to the AP α-subunit — it is this domain that replaces one α-subunit in the M disc (see above). The PB domain is interrupted by the PB-loop, which is about 50 to 65 residues long, depending on the organism [19]. The PB domain of the L_{CM} is thus regarded as one of the core subunits with its PB-loop protruding from the PBS core. Assembly and function of the core can occur in the absence of the PB-loop, leading to a model in which this loop is floating on one side of the PBS, at the membrane surface [20]. Finally, it has been proposed that the domain of L_{CM} called arm2 may be responsible for attachment of the core to the membrane [20].

As mentioned above, the number of PBS core cylinders varies according to the organism. EM studies indicate that each cylinder has a diameter of about 110 Å while its length is given by the stacking of two to four discs of thickness ~30 Å. Additional cylinders called rods radiate upwards from the core structure. The diameter of the discs making up a rod is comparable to those of the core discs – 110 to 120 Å – but their thickness is typically about 60 Å, indicating that the basic structural unit is a hexamer. In addition to the variation in core-cylinder arrangement, the number and composition of rods attached to the core can also vary. This number is usually between six and eight, each rod being composed of 2 to 4 discs depending on the species. Both of these parameters strongly influence the PBS morphology. A hexameric phycocyanin (PC) disc is always located at the rod-core linkage position, while the more distal complexes may be PC, phycoerythrocyanin or phycoerythrin, depending on the organism and the growth conditions. EM and biochemical studies have led to a number of models for the structure of the entire PBS, with variation in the arrangements and associations of rods, and between rods and the core [21]. One of the most popular models of the hemi-discoidal PBS has rods radiating out from the core with approximately even spacing [22,23]. PBSs from several cyanobacterial strains can also contain 1 to 2 molecules of the enzyme Ferredoxin:$NADP^+$ oxidoreductase (FNR) [24,25]. This enzyme catalyses electron transfer between ferredoxin and NADP. In *Synechocystis* sp. strain PCC 6803, two FNR isoforms are present: FNR_S, similar in size to the plastid FNR; and FNR_L, containing an extra N-terminal domain, which is similar to the 10 kDa rod-linker, CpcD (or L_R^{10}). This domain is responsible for FNR binding to the PBS rods [25], and the FNR_L isoform is present in most PBS-containing cyanobacteria. There is, however, some controversy over the location of FNR_L binding — to the PC rod discs proximal [25] or distal [26] to the core.

In this paper we have used EM in combination with single particle averaging to examine negatively-stained PBS particles from WT *Synechocystis* as well as from a number of mutant strains. Firstly the CK mutant was used, in which the PBSs lack PC rods and do not bind FNR (Ughy and Ajlani, unpublished). Secondly the CB mutant was exploited, where PBSs contain only one PC hexamer per rod but retain FNR_L in amounts similar to the wild type [27]. We also examined CBFS [28], having CB-like PBSs (one PC hexamer per rod) but without FNR_L. Finally recombinant FNR_L was reconstituted back into this latter PBS *in vitro*. In the best two-dimensional projection maps of truncated PBS, a resolution of 13 Å was achieved and new densities were observed that could mediate interaction of the cores with the membrane. By comparison of images of PBSs

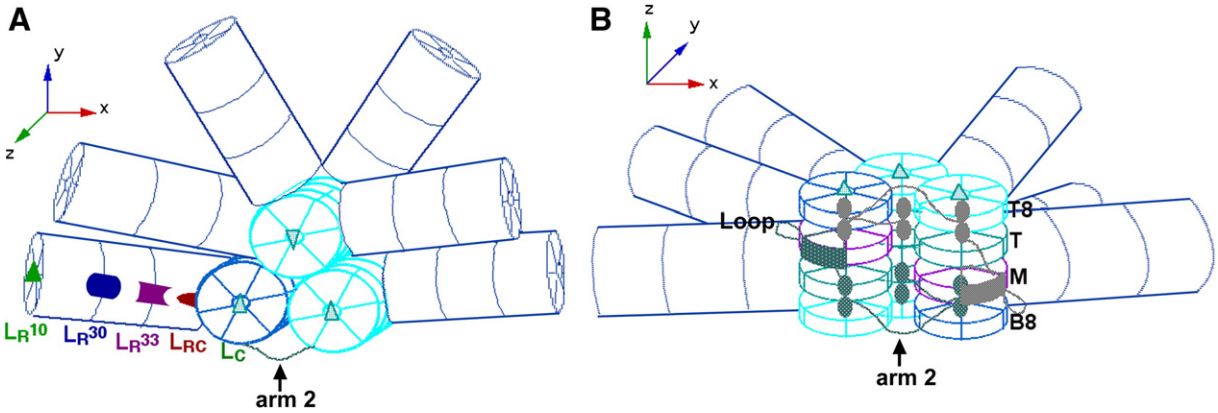

Fig. 1. Representation of a hemi-discoidal PBS, as seen from side (A) and from the thylakoid membrane upwards (B). The architecture exhibits a tri-cylindrical core, from which radiate six rods composed of three PC hexamers each. Differential colouring is used for the subunits of the 3 core cylinders in (B), to illustrate their structural organisation. The 2 core-membrane linkers L_{CM} are represented, with their different domains: the PB-domain (forming part of the M discs), the PB-loop, arm2, and the Reps (filled ellipses). Triangles represent the small core and rod linkers L_C and L_R^{10} respectively.

with and without FNR, we suggest a possible localisation of FNR within the PBS.

2. Materials and methods

2.1. Bacterial growth conditions

Wild-type and mutant strains of the cyanobacterium *Synechocystis* sp. strain PCC 6803 were grown photoautotrophically in modified Allen's medium in an illuminated orbital incubator at 32 °C, in a CO_2-enriched atmosphere and under continuous light (40 μE m^{-2} s^{-1}) [27,29].

2.2. PBS isolation and analysis

Cells were broken by vortexing with glass beads. PBSs were prepared from *Synechocystis* sp. strain 6803 as described in [30,31]. Proteins were analysed by SDS-polyacrylamide gel electrophoresis on 12% Tris–Tricine gels. The OD at 620 nm was used to ensure approximately equal loading of different PBS samples; about 0.3 ODmL at 620 nm (100 μl at OD620 = 3 ≈ 100 μg of protein) was loaded per well. PBS-containing samples were concentrated by precipitation with 10% (v/v) trichloroacetic acid prior to loading. Proteins were visualized using Coomassie blue stain. Recombinant FNR_L (a gift from Dr. B. Lagoutte) was used in reconstitution experiments, performed as in [26], with PBS from the CBFS strain.

2.3. Transmission electron microscopy and image analysis

PBS preparations were negatively stained with 2% uranyl acetate by the droplet method, after glutaraldehyde fixation. Drops of about 5 μL, containing the samples at 0.05 OD in 1 M potassium phosphate pH 8 were deposited on the surface of glow-discharged and carbon-coated copper grids. After 1 min the drop was removed and the grid washed with the same buffer. Then a 5 μL drop of 0.5% glutaraldehyde in 900 mM potassium phosphate was added to the residual material. After 5 min fixation, the drop was washed 3 times in ammonium acetate buffers (500, 50 and 10 mM, respectively), and stained with 2% uranyl acetate.

Electron microscopy was performed on a Philips CM120 electron microscope (FEI, Eindhoven, The Netherlands) operated at 120 kV. Images were recorded under low dose conditions (a total dose ~25 $e^-/Å^2$) with a 4000 SP 4 K slow-scan camera (Gatan, Pleasanton, CA) at −390 nm defocus and at a magnification of 80,000. The pixel size (after binning the images) was 3.75 Å at the specimen level and GRACE software was used for semi-automated specimen selection and data acquisition [32]. In total, from each sample about 1500 images were recorded and 15,000 single particle projections were selected for image analysis. Single-particle analysis was performed with the Groningen Image Processing software package (GRIP) on a PC cluster. Selected single-particle projections were aligned by multi-reference and reference-free alignment procedures [33,34]. Particles were then subjected to multivariate statistical analysis followed by hierarchical classification [34]. Resolution was measured using Fourier-ring correlation and the 3σ criterion [35].

3. Results

Different PBS samples from *Synechocystis* were purified and analysed using the single particle EM technique. Purified PBS complexes usually dissociate, unless high concentrations of phosphate are present. However, high phosphate concentrations interfere with the standard negative staining of samples for EM and often lead to noisy backgrounds. A fixation procedure is therefore required in order to remove phosphate before staining. For this reason, the purified complexes were stabilised with glutaraldehyde on carbon-coated electron microscope grids prior to negative staining, as described in more detail in [36].

3.1. Purification and image analysis of core particles

The isolation of intact core complexes from native PBSs is not feasible because AP trimers dissociate from the core before all rod PC hexamers are detached. Therefore we used the *Synechocystis* CK mutant, totally devoid of PC but still assembling intact core complexes as judged by SDS-PAGE (Fig. 2) and by absorption spectroscopy (Ughy and Ajlani, unpublished). Sucrose gradients of core preparations from the CK mutant contained a unique turquoise band at a significantly higher position than the dark-blue band found for wild-type PBSs. Diluted samples of the turquoise fraction were immediately used to prepare EM grids. Electron micrographs of CK particles show two preferential orientations (top and side views) and a high homogeneity of the sample (Fig. 3). Image analysis of a set of 10,882 negatively-stained particles indicated that the cores were all intact particles without any fragments.

Statistical analysis and classification gave different projection views, presented in Fig. 4A–E. The side-view projections show that the core complex is composed of three cylinders positioned in a regular triangle with a maximal size of 210–220 Å, each of the three sub-domains having a diameter of 110–117 Å (Fig. 4A–C). The X-ray structure of a single AP trimer exhibits clear three-fold symmetry [37]. This symmetry is not observed in the individual AP core cylinders in Fig. 4A, in contrast to EM projection maps of single rod hexamers (Fig. 5Q). This indicates that the position of the AP trimers associated with each cylinder may be translationally-shifted in a direction perpendicular to the long axis of the cylinder. In Fig. 4B, C and D the 2D map of the triangular core particle deviates increasingly from its overall three-fold symmetry, indicating further tilting of the whole particles on the carbon support film. Finally, it should be remarked that the side-view maps of Fig. 4A–C clearly show densities in the centre of the core cylinders. These additional densities probably correspond to the linker proteins connecting the trimers in each core cylinder.

Top views of the particles indicate that the three core cylinders are in an overlap position, with only the outer portions of the two

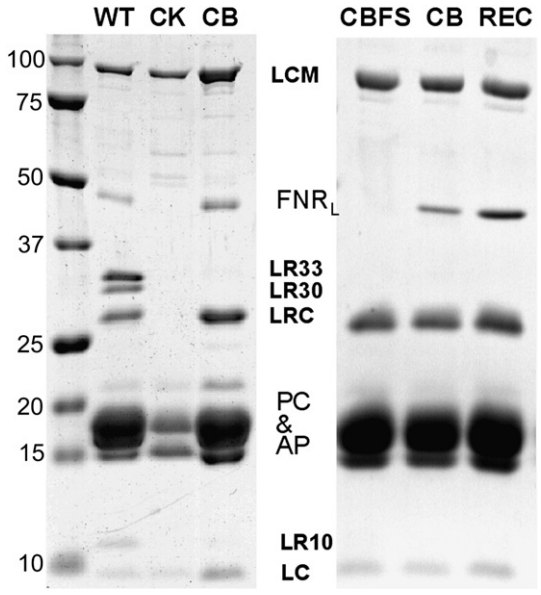

Fig. 2. Polypeptide composition of PBS particles from wild type *Synechocystis* (WT), from mutant strains CK, CB and CBFS, and for CBFS particles reconstituted with FNR (REC). Polypeptide identities are given in the middle; masses of molecular markers are indicated in kDa on the left.

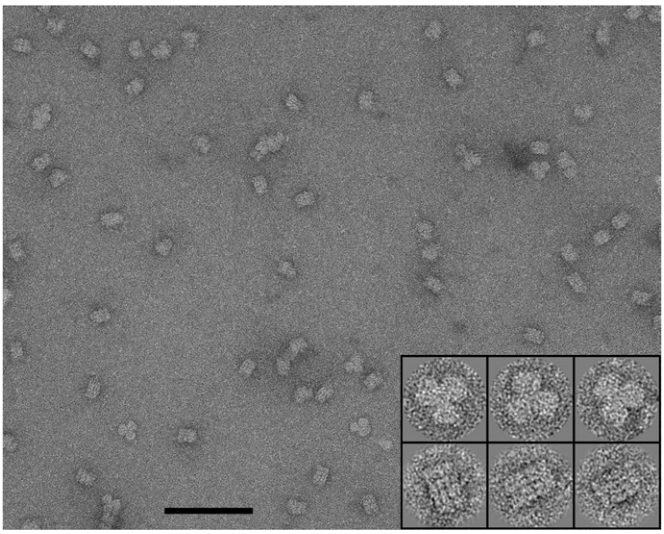

Fig. 3. Electron micrograph of negatively-stained core particles isolated from the CK mutant. Two preferential orientations (side and top views) are observed. The inset shows some enlarged side views (upper row) and top views (lower row). The space bar equals 1000 Å.

lower cylinders visible either side of the upper one (Fig. 4E). The overall dimensions of the core complex, in this position, are about 155 Å wide by 220 Å long. From the staining pattern it appears that the core cylinders of *Synechocystis* are each composed of four AP discs of about 30 Å each. The staining profile also indicates a loose interaction between AP trimers compared with the staining profile within PC hexamers. It is obvious that the stain layer penetrates more deeply between the AP trimers than in the PC hexamer, the latter appearing as a single disc in all our projections (see Fig. 5). The 2D EM map shows that the core has a strong two-fold rotational symmetry in the top-view projection (Fig. 4E). This indicates that the lower two cylinders are arranged in an anti-parallel manner. The two-fold rotational symmetry is also strong in the central parts of the complex where the upper cylinder contributes, implying that the upper cylinder also has internal two-fold symmetry. The symmetry and the absence of tilted particles in the top views suggest that the core particles are probably oriented on the EM grids with their lower (membrane-facing) cylinders towards the carbon film. Since the film surface is negatively charged after glow discharge, interaction with arm2 of the L_{CM} (known to be composed of basic amino acids) might well be responsible for this specific orientation of the core particles.

3.2. Analysis of PBS with shortened PC rods

Attempts to average images of wild-type PBSs yielded poor quality maps (see Fig. 5P), probably due to the inherent instability and flexibility of the rods. To avoid these problems we used the *Synechocystis* CB mutant, in which the lack of two rod-linker proteins (L_R^{33} and L_R^{30}) results in truncated PBSs containing only one PC hexamer per rod (instead of three in the wild type). This mutant retained FNR_L at close to wild type levels [27]. Diluted samples of the dark blue PBS fractions from CB were immediately used to prepare EM grids. Two-dimensional projection maps of negatively-stained particles are presented in Fig. 5A–D. The side-view map of Fig. 5A shows the attachment of six shortened rods to the core; each of the shortened rods is composed of a disc having the dimensions of a single PC hexamer. In addition, some CB particles were missing one or more PC hexamers (~1% of the side views), due either to low stability or to the EM specimen preparation procedure [38]. Thus in Fig. 5B, all three hexamers on the right-hand side of the complex are absent. The core substructure in the CB PBS has a slightly better resolution than that of CK (Fig. 4A), as alignment is improved for the less-symmetrical particles. The map shows two extra masses visible at the base of the complex (green arrows; Fig. 5A, E and I), which may correspond to less well-defined densities in the equivalent positions for the lower resolution map in Fig. 4A. A possible candidate for these masses is arm2 of the L_{CM}, as discussed below.

The projection maps of the untilted top view (Fig. 5C) and a slightly tilted top view (Fig. 5D) are 60 Å longer on each side than the core complex (Fig. 4E) due to the presence of one PC hexamer on each side of the core.

3.3. Relative position of PC rods on the core complexes

The side-views of the CB, CBFS and FNR-reconstituted CBFS particles show six PC hexamers in side-view position (Fig. 5A, E–F, I–J respectively). The staining pattern, however, is not equally strong for all of them with some PC hexamers appearing much darker. In general, the negative staining technique applied to large protein complexes often does not lead to complete embedding in a homogeneous layer of stain from bottom to top of the structure. Instead, the lower parts of a macromolecule, in close contact with the carbon support film, are stronger stain-embedded than the upper parts. As a result, lower parts of a structure appear darker in a 2D-projection map. As exemplified in Fig. 5J, but also visible in Fig. 5A, E, F, I, K, we can see that two out of six hexamers appear significantly darker, as indicated by dark versus bright blue rectangles in Fig. 5J. This indicates that the six different rods are not all in the same plane. In the case of an ideal hemi-discoidal structure they would all have been on the long axis through the centre of the core substructure. The relative positions are difficult to quantify because in the top-view maps the PC rods partly overlap. However, the outer ones at the base of the structure do not overlap for more than half the surface and the maps show that there are no clear displacements in the lower two hexamers 1 and 6 (Fig. 5D; see Fig. 5J for numbering). Thus, most of the displacement is in the two pairs of upper rods (2–5 and 3–4), i.e. those which appear to be attached to the upper core cylinder.

3.4. Searching for the FNR

The position of FNR molecules was studied by analysing two new types of PBS preparation: from the CBFS double mutant, in which

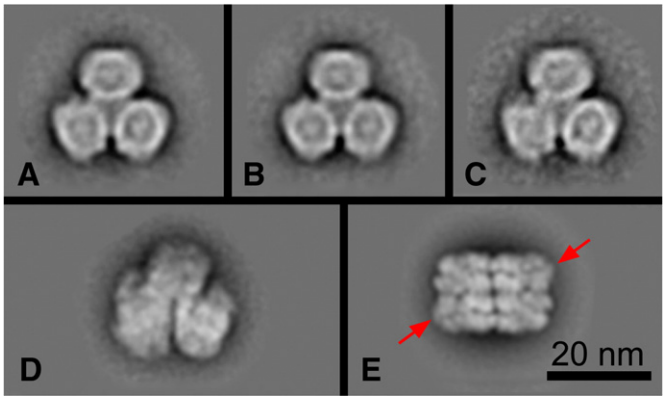

Fig. 4. Single particle analysis of negatively-stained CK particles. The three AP cylinders typical of tri-cylindrical cores are clearly distinguishable in all side views. (A–C) Side-view projections of the cores obtained after image analysis of 9500 particles, with a resolution of 17 Å; (D) Tilted side-view projection generated by a class of 1382 single projections, with a resolution of 21 Å; (E) Top-view projection of the cores obtained from a data set of 5019 particles with a resolution of 13 Å. Red arrows indicate extra densities at the lower left and upper right edges of the particle (see text). No symmetry was imposed during or after image analysis.

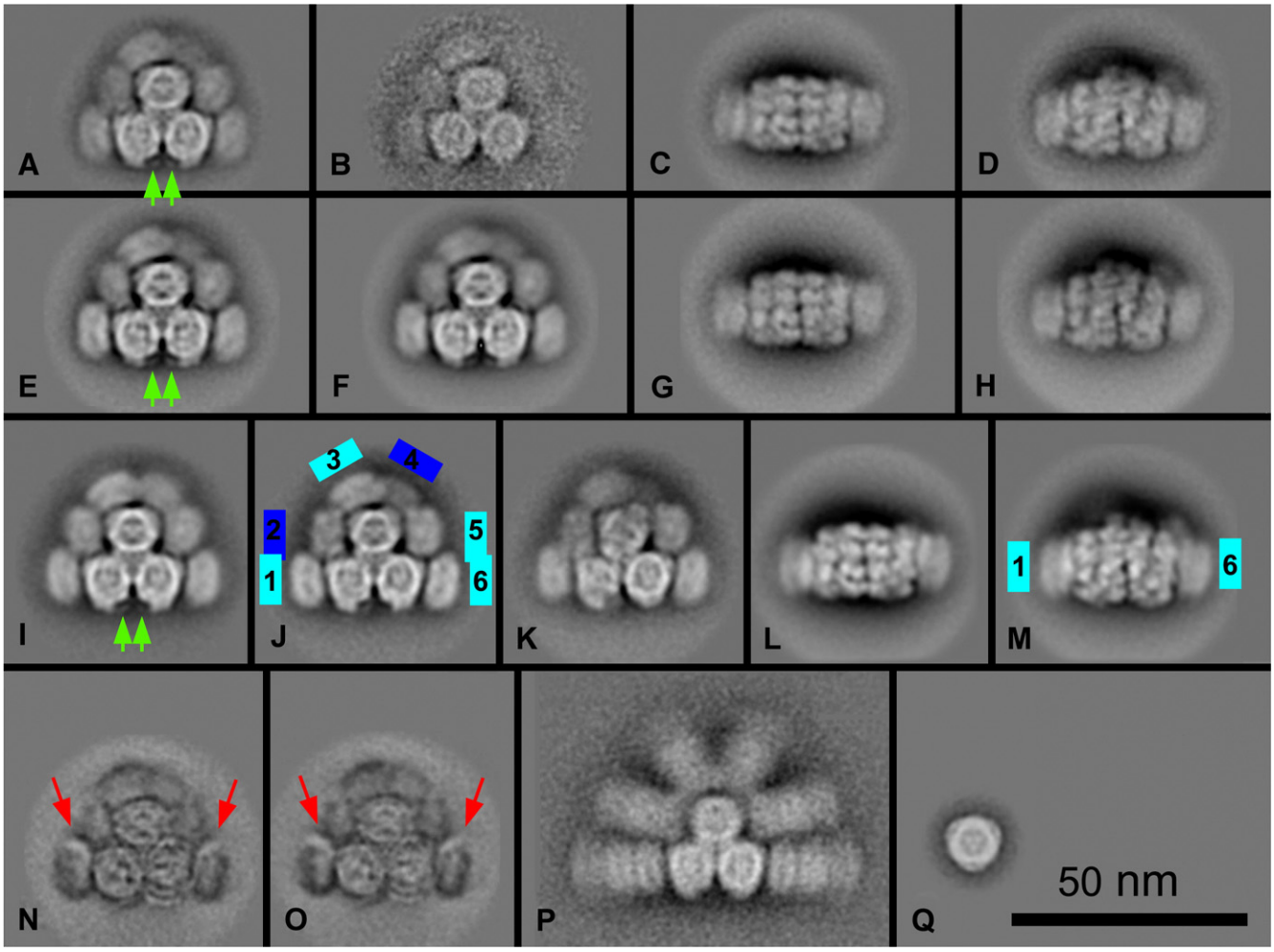

Fig. 5. Gallery of single particle EM images of *Synechocystis* phycobilisomes. No symmetry was imposed on any of the images. Green arrows indicate small densities at the lower side of the AP core, which might play a role in membrane attachment. Light and dark blue rectangles illustrate positional differences of PC rods in side-views of truncated PBSs (see text). Red arrows indicate the major differences in density between particles containing FNR and those without. (A–D) Averaged images of different PBS projections for CB, where the rods are restricted to only one PC hexamer each and where FNR_L is present; (A) Side-view map obtained after a conditional sum of 4695 single particles, with a resolution of 14 Å; (B) Side-view of a partially-disrupted particle, from a separate class of 934 individual particles; (C) Top-view of averaged PBSs from a data set of 1675 single particles at 18 Å resolution; (D) Tilted top-view at 22 Å resolution of averaged PBSs from a data set of 1938 single particles. (E–H) Averaged images of CBFS particles, corresponding to CB without FNR. (E) Side-view projection after image analysis of 2763 particles, at 13 Å resolution; (F) Slightly tilted side-view projection from 2150 particles, with a resolution of 16 Å; (G) Top-view projection after processing of 1758 particles, at 13 Å resolution; (H) Tilted top-view from a data set of 1440 particles, at 16 Å resolution. (I–M) 2D-projections of the REC particle, obtained using CBFS in which FNR was reconstituted *in vitro*. A data set of 6619 single side-view projections of REC PBS was collected; (I) represents the side view, at 13 Å resolution, while (J–K) are slightly-tilted side-view projections at 15 and 20 Å resolution, respectively. A separate data of 6607 single particles was analysed in order to obtain top views of FNR-reconstituted PBS: (L) Top-view projection at 16 Å resolution; (M) slightly-tilted top-view projection at 16 Å resolution. (N) Difference map (I) minus (E); (O) difference map (I) minus (F). (P) Average of 684 side-view projections of the wild-type PBS; (Q) Sum of the PBS rod fragments in top view.

the truncated CB PBS lacks FNR (Fig. 5E–H); and CBFS PBS reconstituted with FNR *in vitro* by the procedure described in [26] (REC; Fig. 5I–M). Fig. 2 shows the polypeptide composition of the PBSs used in this study. Both types of particle exhibit features from the side- and top-view projection maps that are very similar to those of the CB mutant (Fig. 5A–D). The side-view maps have the same 13 Å resolution — note that the small densities at the lower periphery in the side-views are again resolved (green arrows, Fig. 5A, E, I).

A good indication of the position of FNR can be obtained by difference mapping of particles with and without FNR in identical top- or side-view positions. In such maps strong positive densities will indicate the position(s) of FNR. The side-views are the best maps for comparison because they show the least overlap of components such as the PC hexamers. The resulting difference maps (CB-minus-CBFS, REC-minus-CBFS) are shown in Fig. 5N, O for (5I-minus-5E) and (5I-minus-5F), respectively. The strongest difference is at a position between the two phycocyanin rods closest to the membrane (red arrows, Fig. 5N, O). There are no significant differences at the positions of the upper two PC hexamers.

4. Discussion

4.1. Structural features of the phycobilisome

This EM analysis constitutes the first direct structural description of how the core cylinders are associated, and extends the models of the PBS core obtained following core dissociation experiments [15,39]. In these models it was suggested that the core cylinders would differentiate into type A and type B, so that two cylinders of type A and one of type B form a three-cylinder core. Only the two type-A cylinders, each composed of four different discs and a major part of the L_{CM}, would interact with the membrane and the reaction centres within it since the bi-cylindrical core family is restricted to two type-A cylinders [23]. Our EM analysis of truncated PBSs of *Synechocystis* 6803 has resulted in 2D maps to 13 Å resolution,

providing new details of the overall structure and association of core cylinders and PC rods. The projection map of core particles in the top view shows how the four AP discs are arranged in the core substructure. Our data indicate that the two lower cylinders are arranged anti-parallel and that the upper cylinder also exhibits an internal two-fold symmetry (see Fig. 1).

It has been shown by site-directed mutagenesis that the PB-loop domain of the L_{CM} does not play a role in PBS anchoring and should therefore be at the outer side of the basal (type-A) cylinders of the core [20]. Small densities at the top right and bottom left of the core top-view in Fig. 4E (indicated by red arrows) could be the positions of the PB-loops of the two L_{CM} polypeptides present in the core.

The fact that the top-view 2D projections of the cores replicate the two-fold symmetry of the 3D model indicates that the particles are oriented on the grids with their lower cylinders towards the negatively charged carbon film. We propose that the novel densities, revealed at the bottom of the two lower cylinders in the side-view maps (green arrows, Fig. 5A, E, I), correspond to the arm2 domain of the L_{CM} linker. This domain has been proposed to play a role in anchoring of the PBS to the thylakoid membrane [20]. Since arm2 of the L_{CM} is known to be composed principally of basic amino acids, electrostatic interaction between PBS and the photosystems might occur *in vivo* since the presence of phospholipids and sulpholipids gives a partial negative charge to the membrane surface. Six negatively charged lipids are found exclusively at the cytoplasmic side of the PSII dimer [40], which may play a role in PBS anchoring. On the other hand, a PSI trimer contains less negatively charged lipids that are buried between the monomers or under the peripheral subunits [41]. Thus electrostatic interaction might occur between PSII and the PBS. Moreover, the overall symmetry and dimension of the core match those of the PSII dimer, while they do not match those of PSI. Furthermore, the PSII cytoplasmic surface is flat and could accommodate a PBS on its top. It would be difficult to imagine anything similar for PSI cytoplasmic surface, which contains peripheral subunits (see also last paragraph).

The top view image of the cores revealed a rotational two-fold symmetry that confirms the antiparallel model for the basal cylinders proposed by Glazer for the bi-cylindrical cores of *Synechococcus* [17]. For the bi-cylindrical core, this symmetry can be obtained whatever the orientation of AP trimers within the cylinder is. The two-fold rotational symmetry found in our tri-cylindrical samples implies that at least in the upper cylinder, two types of interaction exist between the four AP trimers, i.e. a face-to-face interaction between the T8 and T discs and a face-to-back one between the two central T discs (Fig. 1). T8 and T also constitute half of the basal cylinder and their interaction must be similar to that in the upper cylinder. We propose that the basal cylinders have a similar disc organisation except for the replacement of T8–T trimers by B8–M trimers. This organisation is similar to that found in the rods, where PC trimers are known to aggregate face-to-face to form a tight hexamer that is further assembled face-to-back into rods by the rod linkers.

During image analysis of the WT PBS sample, we observed an abundance of smaller particles at the level of the micrograph. After separate image analysis, an average projection of these smaller particles is shown in Fig. 5Q. This view, which could represent individual PC hexamers, shows a central mass composed of three small protein densities. Three similar small densities are visible in the face view of the upper core cylinder (Fig. 4 A, B), while they are not seen in the lower two ones. This may indicate that the lower cylinders do not make the same angle as the upper one in respect to a hypothetical axis along the centre of the three cylinders. Alternatively there may be different linkers present in the lower two AP cylinders.

The WT PBS is not only a large structure but appears to be rather flexible as well, as averaged projection maps appear fuzzy, particularly towards the ends of the rods (Fig. 5P). In contrast, the maps of rod-truncated PBSs show well-preserved details, up to about 13–14 Å in the best maps (Fig. 5A, E, I). The negative stain distribution in the averaged side views indicates that not all the rods have the same position where they bind to the core. On the other hand, the top view does not show any substantial displacements in the lower two hexamers 1 and 6 (Fig. 5D; numbering in Fig. 5J). Rods 2 and 4, coloured dark blue in Fig. 5J, appear to be displaced. Because the core structure exhibits two-fold symmetry, the position of the six rods is related by the same two-fold rotational symmetry. This allows us to propose a consistent model with displacements as indicated in Fig. 6. Rods 2 and 3 are shifted outward in opposite directions, but because rods 5 and 4 are related by symmetry then these must be at the same off-axis position as rods 2 and 3, respectively. Unfortunately, the top views of these particles do not give further clues about the displacements of the rods, mainly because they overlap with the core structure.

4.2. Localising the FNR

In our attempts to assign the location of FNR we examined truncated PBSs for three different types of particle: (1) from the CB mutant, which contains FNR_L; (2) from the FNR_L-lacking CBFS mutant; and (3) CBFS PBS with reconstituted FNR (called REC). The projection

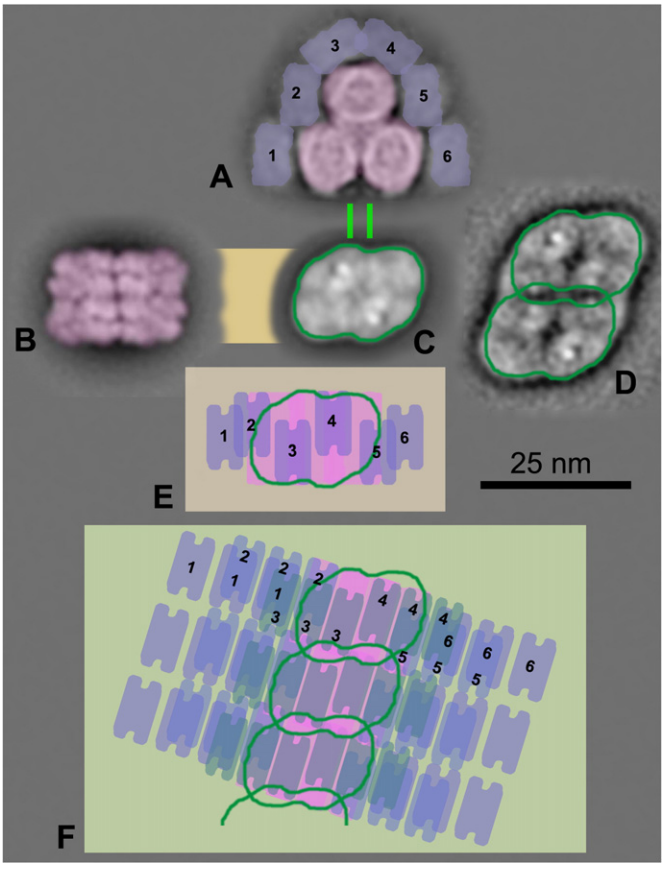

Fig. 6. Schematic model for the interaction of PBSs with PSII rows in *Synechocystis*. Side-view projection of PBS containing only one PC hexamer per rod (core in pink and rods in blue). Light green bars indicate small densities at the lower side of the core, which might play a role in PBS membrane association via PSII subunits (note alignment with dimer in C). (B) Top-view of the *Synechocystis* core indicates that it matches the width of the cyanobacterial PSII dimer (C) and double dimer (D). PSII dimer is outlined in dark green. (E) Schematic arrangement of a single truncated PBS over a single PSII dimer, seen in top view from the stromal side of the membrane. Numbers 1 to 6 (in blue) indicate positions of the corresponding PC hexamers from (A). (F) Final model, viewed from the stromal side of the membrane, indicates the most likely arrangement of WT PBSs on PSII rows. Numbers 1-1-1 to 6-6-6 indicate positions of the three PC discks within each of the six rods (in blue).

maps show similar resolution for CB, CBFS and REC samples, so that the small densities at the lower periphery of the side-views, assigned to arm2 of the L_{CM}, have been resolved in all three particles. By subtracting the projections in which FNR is not present from those where it is, difference maps were generated to see possible positions of FNR. The best maps were produced by comparing the REC particle with the CBFS PBS. A positive density is revealed at two symmetry-related positions (Fig. 5N, O), as marked by red arrows. It suggests the position of at least two FNR molecules. This position is at the interface of the two lower PC rods, while there is no difference at the position of the upper rods. The fact that we see the difference in Fig. 5N,O at two symmetry-related positions, without having imposed any type of symmetry on images during or after analysis, is good evidence in favor of our FNR assignment.

4.3. Arrangement on photosystem II rows

About 20 years ago freeze-fracture EM convincingly revealed that EF particles (PSII dimers) in PBS-containing organisms could be either randomly distributed (in high light or state 2) or organised into rows (in low light or state 1). The spacing between the EF particles in the row was about 120 Å [42,43]. The periodicity of the particles in a row is compatible with the width of a PBS core, while the distance between the rows is proportional to the length of the PBS. In *Synechocystis* thylakoids adapted to state 1, the distance between the rows is 500 Å in the wild type, 230 Å in a rod-less mutant and 160 Å in a PBS-less mutant [44]. Similar distances between PSII were obtained by single particle analysis based on negatively-stained specimens of solubilised thylakoids, by measuring centre-to-centre distances between dimers in the PSII double dimer [43]. A periodicity of 122 Å and an inter-row distance of 167 Å were obtained by Folea et al. [45].

Our PBS top-view projections indicate that the core is about 155 Å in width (by 220 Å long), a similar but slightly larger width than dimeric PSII (140 Å by 200 Å) [46]. This is of interest because it would mean that a 1:1 matching of PBSs on the top of PSII rows is only possible when the PBSs make a lateral angle of about 17° with the PSII row, as indicated in our model. The model shows how the two-fold symmetrical PBSs would fit on top of rows of dimeric PSII, and refines previous models for the relative position and attachment of PBS over PSII rows. In our model the PBS is in contact with its neighbours on adjacent PSII molecules in a row, in particular via the displaced PC rods 2 and 5, which might redistribute excitation energy between these giant extra-membranous antennae, thus optimising light harvesting for PSII.

The model presented above represents the best fit of existing 2D electron projection data, but it is still based partly on indirect observations. Up to now, no PSII complex with an associated PBS has ever been characterised by EM and attempts to purify such complexes give inconsistent results [47–49]. The exact position of the PBS on PSII thus remains to be determined. The instability of the PSII–PBS complex is a major drawback for its characterisation. One way to improve stability would be to construct specific cysteine mutants within PSII and PBS subunits. They could then be cross-linked via disulphide bridges to give a megacomplex with higher stability.

Acknowledgements

We thank B. Lagoutte for the generous gift of recombinant FNR_L, B. Robert for his support and A. Pascal for critical reading of the manuscript. G. Oostergetel, W. Keegstra and J.-M. Verbavatz are acknowledged for invaluable help with electron microscopy and image processing. This project is part of the Dutch research programme “From Molecule to Cell” funded by the Netherlands Organization for Scientific Research (NWO) and the Foundation for Earth and Life Sciences (ALW). Work in GA's lab was financially supported by the CNRS, the CEA, and the research programme ANR-PhycoSyn.

This paper is dedicated to Claudie Vernotte.

References

[1] A.N. Glazer, Light guides. Directional energy transfer in a photosynthetic antenna, J. Biol. Chem. 264 (1989) 1–4.
[2] M.H. Yu, A.N. Glazer, Cyanobacterial phycobilisomes. Role of the linker polypeptides in the assembly of phycocyanin, J. Biol. Chem. 257 (1982) 3429–3433.
[3] T. Schirmer, R. Huber, M. Schneider, W. Bode, M. Miller, M.L. Hackert, Crystal structure analysis and refinement at 2.5 Å of hexameric C-phycocyanin from the cyanobacterium *Agmenellum quadruplicatum*, J. Mol. Biol. 188 (1986) 651–676.
[4] J.Y. Liu, T. Jiang, J.P. Zhang, D.C. Liang, Crystal structure of allophycocyanin from red algae *Porphyra yezoensis* at 2.2-A resolution, J. Biol. Chem. 274 (1999) 16945–16952.
[5] J. Nield, P.J. Rizkallah, J. Barber, N.E. Chayen, The 1.45 Å three-dimensional structure of C-phycocyanin from the thermophilic cyanobacterium *Synechococcus elongatus*, J. Struct. Biol. 141 (2003) 149–155.
[6] W.A. Sidler, Phycobilisome and phycobiliprotein structures, In: DA Bryant (Ed.), The Molecular Biology of Cyanobacteria, Kluwer Acad. Pub., Dordrecht, 1994, pp. 139–216.
[7] E. Gantt, C.A. Lipschultz, Phycobilisomes of *Porphyridium cruentum*. I. Isolation, J. Cell Biol. 54 (1972) 313–324.
[8] G. Guglielmi, G. Cohen-Bazire, D.A. Bryant, The structure of *Gleobacter violaceus* and its phycobilisome, Arch. Microbiol. 129 (1981) 181–189.
[9] D.W. Krogmann, B. Perez-Gomez, E.B. Gutierrez-Cirlos, A. Chagolla-Lopez, L. Gonzalez de la Vara, C. Gomez-Lojero, The presence of multidomain linkers determines the bundle-shape structure of the phycobilisome of the cyanobacterium *Gloeobacter violaceus* PCC 7421, Photosynth. Res. 93 (2007) 27–43.
[10] G. Yamanaka, A.N. Glazer, R.C. Williams, Molecular architecture of a light-harvesting antenna. Comparison of wild type and mutant *Synechococcus* 6301 phycobilisomes, J. Biol. Chem. 255 (1980) 11104–11110.
[11] D.A. Bryant, R. de Lorimier, G. Guglielmi, S.E. Stevens Jr., Structural and compositional analyses of the phycobilisomes of *Synechococcus* sp. PCC 7002. Analyses of the wild-type strain and a phycocyanin-less mutant constructed by interposon mutagenesis, Arch. Microbiol. 153 (1990) 550–560.
[12] R.C. Williams, J.C. Gingrich, A.N. Glazer, Cyanobacterial phycobilisomes. Particles from *Synechocystis* 6701 and two pigment mutants, J. Cell Biol. 85 (1980) 558–566.
[13] K. Elmorjani, J.-C. Thomas, P. Sebban, Phycobilisomes of wild type and pigment mutants of the cyanobacterium *Synechocystis* PCC 6803, Arch. Microbiol. 146 (1986) 186–191.
[14] D. Redecker, W. Wehrmeyer, W. Reuter, Core substructure of the hemiellipsoidal phycobilisome from the red alga *Porphyridium cruentum*, Eur. J. Cell Biol. 62 (1993) 442–450.
[15] A. Ducret, S.A. Muller, K.N. Goldie, A. Hefti, W.A. Sidler, H. Zuber, A. Engel, Reconstitution, characterisation and mass analysis of the pentacylindrical allophycocyanin core complex from the cyanobacterium *Anabaena* sp. PCC 7120, J. Mol. Biol. 278 (1998) 369–388.
[16] M. Glauser, D.A. Bryant, G. Frank, E. Wehrli, S.S. Rusconi, W. Sidler, H. Zuber, Phycobilisome structure in the cyanobacteria *Mastigocladus laminosus* and *Anabaena* sp. PCC 7120, Eur. J. Biochem. 205 (1992) 907–915.
[17] D.J. Lundell, A.N. Glazer, Molecular architecture of a light-harvesting antenna. Core substructure in *Synechococcus* 6301 phycobilisomes: two new allophycocyanin and allophycocyanin B complexes, J. Biol. Chem. 258 (1983) 902–908.
[18] D.A. Bryant, Genetic analysis of phycobilisome biosynthesis, assembly, structure, and function in the cyanobacterium *Synecococcus* sp PCC 7002, In: SE Stevens Jr., DA Bryant (Eds.), Light-Energy Transduction in Photosynthesis: Higher Plants and Bacterial Models, American Society of Plant Physiologists, Rockville, 1988, pp. 62–90.
[19] V. Capuano, A. Braux, N. Tandeau de Marsac, J. Houmard, The “anchor polypeptide” of cyanobacterial phycobilisomes. Molecular characterization of the *Synechococcus sp.* PCC 6301 *apcE* gene. J. Biol. Chem. 266 (1991) 7239–7247.
[20] G. Ajlani, C. Vernotte, Deletion of the PB-loop in the L_{CM} subunit does not affect phycobilisome assembly or energy transfer functions in the cyanobacterium *Synechocystis* sp. PCC6714, Eur. J. Biochem. 257 (1998) 154–159.
[21] N. Adir, Elucidation of the molecular structures of components of the phycobilisome: reconstructing a giant, Photosynth. Res. 85 (2005) 15–32.
[22] R. MacColl, Cyanobacterial phycobilisomes, J. Struct. Biol 124 (1998) 311–334.
[23] L.K. Anderson, C.M. Toole, A model for early events in the assembly pathway of cyanobacterial phycobilisomes, Mol. Microbiol. 30 (1998) 467–474.
[24] W.M. Schluchter, D.A. Bryant, Molecular characterization of ferredoxin-$NADP^+$ oxidoreductase in cyanobacteria: cloning and sequence of the *petH* gene of *Synechococcus* sp. PCC 7002 and studies on the gene product, Biochemistry 31 (1992) 3092–3102.
[25] J.J. van Thor, O.W. Gruters, H.C. Matthijs, K.J. Hellingwerf, Localization and function of ferredoxin:NADP(+) reductase bound to the phycobilisomes of *Synechocystis*, EMBO J. 18 (1999) 4128–4136.
[26] C. Gomez-Lojero, B. Perez-Gomez, G. Shen, W.M. Schluchter, D.A. Bryant, Interaction of ferredoxin:$NADP^+$ oxidoreductase with phycobilisomes and phycobilisome substructures of the cyanobacterium *Synechococcus* sp. strain PCC 7002, Biochemistry 42 (2003) 13800–13811.
[27] B. Ughy, G. Ajlani, Phycobilisome rod mutants in *Synechocystis* sp. strain PCC6803, Microbiology 150 (2004) 4147–4156.

[28] J.C. Thomas, B. Ughy, B. Lagoutte, G. Ajlani, A second isoform of the ferredoxin: NADP oxidoreductase generated by an in-frame initiation of translation, Proc. Natl. Acad. Sci. U. S. A. 103 (2006) 18368–18373.
[29] M.M. Allen, Simple conditions for growth of unicellular blue-green algae on plates. J. Phycol. 4 (1968) 1–4.
[30] A.N. Glazer, Phycobilisomes, Methods Enzymol. 167 (1988) 304–312.
[31] G. Ajlani, C. Vernotte, L. DiMagno, R. Haselkorn, Phycobilisome core mutants of *Synechocystis* PCC 6803, Biochim. Biophys. Acta 1231 (1995) 189–196.
[32] G.T. Oostergetel, W. Keegstra, A. Brisson, Automation of specimen selection and data acquisition for protein electron crystallography, Ultramicroscopy 74 (1998) 47–59.
[33] P. Penczek, M. Radermacher, J. Frank, Three-dimensional reconstruction of single particles embedded in ice, Ultramicroscopy 40 (1992) 33–53.
[34] M. van Heel, B. Gowen, R. Matadeen, E.V. Orlova, R. Finn, T. Pape, D. Cohen, H. Stark, R. Schmidt, M. Schatz, A. Patwardhan, Single-particle electron cryo-microscopy: towards atomic resolution, Q. Rev. Biophys. 33 (2000) 307–369.
[35] M. van Heel, Similarity measures between images, Ultramicroscopy 21 (1987) 95–100.
[36] A.N. Glazer, R.C. Williams, G. Yamanaka, H.K. Schachman, Characterization of cyanobacterial phycobilisomes in zwitterionic detergents, Proc. Natl. Acad. Sci. U S A. 76 (1979) 6162–6166.
[37] K. Brejc, R. Ficner, R. Huber, S. Steinbacher, Isolation, crystallization, crystal structure analysis and refinement of allophycocyanin from the cyanobacterium *Spirulina platensis* at 2.3 Å resolution, J. Mol. Biol. 249 (1995) 424–440.
[38] B. Kastner, N. Fischer, M.M. Golas, B. Sander, P. Dube, D. Boehringer, K. Hartmuth, J. Deckert, F. Hauer, E. Wolf, H. Uchtenhagen, H. Urlaub, F. Herzog, J.M. Peters, D. Poerschke, R. Luhrmann, H. Stark, GraFix: sample preparation for single-particle electron cryomicroscopy, Nat. Methods 5 (2008) 53–55.
[39] L.K. Anderson, F.A. Eiserling, Asymmetrical core structure in phycobilisomes of the cyanobacterium *Synechocystis* 6701, J. Mol. Biol. 191 (1986) 441–451.
[40] B. Loll, J. Kern, W. Saenger, A. Zouni, J. Biesiadka, Lipids in photosystem II: Interactions with protein and cofactors, Biochim. Biophys. Acta 1767 (2007) 509–519.
[41] P. Jordan, P. Fromme, O. Klukas, H.T. Witt, W. Saenger, N. Krau, Three-dimensional structure of cyanobacterial photosystem I at 2.5 Å resolution, Nature 411 (2001) 909–917.
[42] E. Mörchel, M. Schatz, Correlation of photosystem II complexes with exo-plasmatic freeze-fracture particles of thylakoids of the cyanobacterium *Synechococcus* sp. Planta 172 (1987) 145–154.
[43] C. Vernotte, C. Astier, J. Olive, State 1–state 2 adaptation in the cyanobacteria *Synechocystis* PCC 6714 wild type and *Synechocystis* 6803 wild type and phycocyanin-less mutant, Photosynth. Res. 26 (1990) 203–212.
[44] J. Olive, G. Ajlani, C. Astier, M. Recouvreur, C. Vernotte, Ultrastructure and light adaptation of phycobilisome mutants of *Synechocystis* sp. PCC 6803. Biochim. Biophys. Acta 1319 (1997) 275–282.
[45] I.M. Folea, P. Zhang, E.M. Aro, E.J. Boekema, Domain organization of photosystem II in membranes of the cyanobacterium *Synechocystis* PCC6803 investigated by electron microscopy, FEBS Lett. 582 (2008) 1749–1754.
[46] A.A. Arteni, M. Nowaczyk, J. Lax, R. Kouřil, M. Rögner, E.J. Boekema, Single particle electron microscopy in combination with mass spectrometry to investigate novel complexes of membrane proteins, J. Struct. Biol. 149 (2005) 325–331.
[47] J. Clement-Metral, E. Gantt, Isolation of oxygen-evolving phycobilisome-photosystem II particles from *Porphyridium cruentum*, FEBS Lett. 156 (1983) 185–188.
[48] T. Katoh, E. Gantt, Photosynthetic vesicles with bound phycobilisomes from *Anabaena variabilis*, Biochim. Biophys. Acta 546 (1979) 383–393.
[49] C.W. Mullineaux, Phycobilisome-reaction centre interaction in cyanobacteria, Photosynth. Res. 95 (2008) 175–182.